An Improved Adaptive Output Tracking Control for Three-Dimensional Overhead Cranes with Double-Pendulum Effect

Bingqing Zhao and Huimin Ouyang$^{(\boxtimes)}$

College of Electrical Engineering and Control Science, Nanjing Tech University, Nanjing 211816, China
ouyang1982@njtech.edu.cn

Abstract. As a tool for transporting goods, three-dimensional bridge cranes are widely used in many industrial sites, such as workshops, warehouses, docks and so on. The main control objective is to transport goods to the designated position smoothly and quickly while restraining load swing angles. However, the influence of external disturbances and the uncertainty of the system model parameters increase the difficulty of designing the controller. In the first step, we constructed a composite signal to increase the coupling relationship of the state vectors, and then designed an adaptive tracking controller, which can achieve a satisfactory tracking effect while completing the estimations of the uncertain model parameters. In the second step, considering the fact that the velocity signals are not measurable in actual situations, we replace the velocity feedback with velocity-like signals, and then propose an improved adaptive tracking control strategy. Use Matlab as a simulation platform to complete comparative simulation and robustness verification. A series of simulation results shows that the designed controller can complete the control goal and its control performance is significantly better than the other two controllers in the comparative simulation.

Keywords: Three-dimensional overhead crane · Adaptive tracking · Output feedback

1 Introduction

Overhead cranes play a very important role in cargo transfer in industrial sites because of their small footprint, convenience, and fast transportation. As a large-scale mechanical equipment, with the popularization and use of overhead cranes in various industrial environments, higher and higher requirements are put forward for its stable, efficient and safe operation. Therefore, research on crane automation control technology is gradually becoming more important [1].

The crane has a process of acceleration or deceleration during operation, which is bound to cause the swing of load. This kind of swing phenomenon is particularly obvious during the starting and braking of the crane. In addition, overhead crane use hook to connect load during lifting operation, so it

exhibits double pendulum characteristics. When the crane trolley moves to a predetermined position, the swing of the load will cause difficulty in hoisting and positioning, increase the duration of hoisting operations, and lower the work efficiency of the crane. Aiming at the problem of trolley positioning and swing angle suppression, many scholars have provided solutions and optimization strategies, which can be divided into open loop control, and closed loop control. Open loop control includes motion planning optimal control [2–4] and input shaping control [5–7]. Closed-loop control includes sliding mode control [8–10], adaptive control [11–13], passivity-based control [14–16] and intelligent control [17–19].

Then, some typical control strategies are enumerated and analyzed. Fu et al. proposed a minimum time motion online planning method under constrained conditions in [20]. Considering the coupling relationship between trolley positioning and load swing, an optimization problem is proposed and the solution of the motion planning problem is calculated in real time. Taking into account the problem of load assignment of multiple cranes in real work scenarios, Ji et al. created a mixed integer programming in which a mathematical equation can solve the optimization problem. Through case analysis, this method can improve crane transportation efficiency [21]. In order to achieve the control objectives of trolley positioning and anti swing, Zhang et al. designed an online motion planning method in [22]. The proposed method includes the correlation functions of trolley positioning and swing angles, and the effectiveness of the method is verified by theoretical proof and simulation. A disturbance observer control strategy that can eliminate unknown disturbances in finite time is designed by Wu in [23]. During the design process, some conversions were made to the original dynamic model of the crane system. Mathematical analysis and experiments verify the superiority of this method. Combining adaptive control and sliding mode control, an adaptive integral sliding mode controller is derived by Zhang et al. in [24]. At the same time, the purpose of swing angle suppression is achieved by increasing the state vector coupling. In [25], Le et al. designed a hierarchical sliding mode controller based on the crane system, and then used an intelligent algorithm to determine the control gains.

After careful investigation, it is certain that the existing literature provides ideas for the control method of the three-dimensional double pendulum crane system to a large extent. However, some problems still need to be resolved for the crane system studied in this article: (1) Due to the complexity of the three-dimensional double pendulum overhead crane model, it is challenging to design the controller to achieve the control goal. It can be found that in most literatures, when faced with a complex model with many degrees of freedom, the author ignores some nonlinear terms to simplify the model, and then performs controller design or theoretical analysis on the basis of the simplified model. (2) There are often some unknown disturbances in actual working scenarios, and this issue should also be considered when designing the controller. (3) Many existing controllers contain velocity signals, but in reality, the velocity signals are unmeasurable when the crane is hoisting.

Thus, in order to solve the above problems, an improved adaptive tracking controller without velocity feedback is proposed. In summary, the main contributions of this method are as follows: (1) Unlike the traditional controllers, it does not need to linearize the dynamic model of crane system when designing the controller. (2) In practice, there are always unknown external disturbances in the crane system, which is considered in this paper. (3) The problem of unmeasurable velocity and angular velocity is overcome by introducing velocity function.

2 Three-Dimensional Overhead Cranes with Double-Pendulum Modeling and Control Objective

2.1 System Modeling

According to Fig. 1, the dynamic model of the crane can be obtained as follows [26,27].

$$M(q)\ddot{q} + C(q,\dot{q})\dot{q} + G(q) = \Gamma - \Xi \tag{1}$$

The specific expressions of $M(q)$, $C(q,\dot{q})$, $G(q)$ and Γ can be calculated mathematically as follows:

$$M(q) = \begin{bmatrix} m_{11} & m_{12} & m_{13} & m_{14} & m_{15} & m_{16} \\ m_{21} & m_{22} & m_{23} & m_{24} & m_{25} & m_{26} \\ m_{31} & m_{32} & m_{33} & m_{34} & m_{35} & m_{36} \\ m_{41} & m_{42} & m_{43} & m_{44} & m_{45} & m_{46} \\ m_{51} & m_{52} & m_{53} & m_{54} & m_{55} & m_{56} \\ m_{61} & m_{62} & m_{63} & m_{64} & m_{65} & m_{66} \end{bmatrix}, C(q,\dot{q}) = \begin{bmatrix} c_{11} & c_{12} & c_{13} & c_{14} & c_{15} & c_{16} \\ c_{21} & c_{22} & c_{23} & c_{24} & c_{25} & c_{26} \\ c_{31} & c_{32} & c_{33} & c_{34} & c_{35} & c_{36} \\ c_{41} & c_{42} & c_{43} & c_{44} & c_{45} & c_{46} \\ c_{51} & c_{52} & c_{53} & c_{54} & c_{55} & c_{56} \\ c_{61} & c_{62} & c_{63} & c_{64} & c_{65} & c_{66} \end{bmatrix},$$

$$G(q) = \begin{bmatrix} 0 & 0 & g_3 & g_4 & g_5 & g_6 \end{bmatrix}^T, \Gamma = \begin{bmatrix} F_x - F_{rx} & F_y - F_{ry} & 0 & 0 & 0 & 0 \end{bmatrix}^T,$$

$$\Xi = \begin{bmatrix} \Xi_1 & \Xi_2 & \Xi_3 & \Xi_4 & \Xi_5 & \Xi_6 \end{bmatrix}^T, q = \begin{bmatrix} x & y & \theta_1 & \theta_2 & \theta_3 & \theta_4 \end{bmatrix}^T,$$

$$m_{11} = M_1 + m_1 + m_2, m_{12} = 0, m_{13} = (m_1 + m_2)l_1C_1C_2,$$

$$m_{14} = -(m_1 + m_2)l_1S_1S_2, m_{15} = m_2l_2C_3C_4, m_{16} = -m_2l_2S_3S_4,$$

$$m_{21} = 0, m_{22} = M_2 + m_1 + m_2, m_{23} = 0, m_{24} = (m_1 + m_2)l_1C_2,$$

$$m_{25} = 0, m_{26} = m_2l_2C_4, m_{31} = (m_1 + m_2)l_1C_1C_2, m_{32} = 0,$$

$$m_{33} = (m_1 + m_2)l_1^2C_2^2, m_{34} = 0, m_{35} = m_2l_1l_2C_{1-3}C_2C_4,$$

$$m_{36} = m_2l_1l_2S_{1-3}C_2S_4, m_{41} = -(m_1 + m_2)l_1S_1S_2,$$

$$m_{42} = (m_1 + m_2)l_1C_2, m_{43} = 0, m_{44} = m_1l_1^2 + m_2l_2^2,$$

$$m_{45} = -m_2l_1l_2S_{1-3}S_2C_4,$$

$$m_{46} = m_2l_1l_2(C_2C_4 + C_1C_3S_2S_4 + S_1S_2S_3S_4),$$

$$m_{51} = m_2l_2C_3C_4, m_{52} = 0, m_{53} = m_2l_1l_2C_{1-3}C_2C_4,$$

$$m_{54} = -m_2l_1l_2S_{1-3}S_2C_4, m_{55} = m_2l_2^2C_4^2, m_{56} = 0,$$

$$m_{61} = -m_2l_2S_3S_4, m_{62} = m_2l_2C_4, m_{63} = m_2l_1l_2S_{1-3}C_2S_4,$$

$$m_{64} = m_2l_1l_2(C_2C_4 + C_1C_3S_2S_4 + S_1S_2S_3S_4), m_{65} = 0, m_{66} = m_2l_2^2$$

$c_{11} = 0, c_{12} = 0, c_{13} = -(m_1 + m_2)l_1(C_2S_1\dot{\theta}_1 + C_1S_2\dot{\theta}_2),$

$c_{14} = -(m_1 + m_2)l_1(C_1S_2\dot{\theta}_1 + C_2S_1\dot{\theta}_2), c_{15} = -m_2l_2(C_4S_3\dot{\theta}_3 + C_3S_4\dot{\theta}_4),$

$c_{16} = -m_2l_2(C_3S_4\dot{\theta}_3 + C_4S_3\dot{\theta}_4), c_{21} = 0, c_{22} = 0, c_{23} = 0,$

$c_{24} = -(m_1 + m_2)l_1 \sin\theta_2\dot{\theta}_2, c_{25} = 0, c_{26} = -m_2l_2 \sin\theta_4\dot{\theta}_4,$

$c_{31} = 0, c_{32} = 0, c_{33} = -(m_1 + m_2)l_1^2 S_2 C_2 \dot{\theta}_2,$

$c_{34} = -(m_1 + m_2)l_1^2 S_2 C_2 \dot{\theta}_1, c_{35} = m_2 l_1 l_2 S_{1-3}(C_2 C_4 \dot{\theta}_3 + S_2 S_4 \dot{\theta}_4),$

$c_{36} = -m_2 l_1 l_2 C_2 (C_1 C_3 S_4 \dot{\theta}_3 + S_1 S_3 S_4 \dot{\theta}_3 + C_1 C_4 S_3 \dot{\theta}_4 - C_3 C_4 S_1 \dot{\theta}_4),$

$c_{41} = 0, c_{42} = 0, c_{43} = (m_1 + m_2)l_1^2 S_2 C_2 \dot{\theta}_1, c_{44} = 0,$

$c_{45} = m_2 l_1 l_2 S_2 (C_1 C_3 C_4 \dot{\theta}_3 + C_4 S_1 S_3 \dot{\theta}_3 - C_1 S_3 S_4 \dot{\theta}_4 + C_3 S_1 S_4 \dot{\theta}_4),$

$c_{46} = m_2 l_1 l_2 (C_1 C_3 C_4 S_2 \dot{\theta}_4 + C_4 S_1 S_2 S_3 \dot{\theta}_4 - C_2 S_4 \dot{\theta}_4 - C_1 S_2 S_3 S_4 \dot{\theta}_3$

$+ C_3 S_1 S_2 S_4 \dot{\theta}_3), c_{51} = 0, c_{52} = 0,$

$c_{53} = -m_2 l_1 l_2 C_4 (C_2 C_3 S_1 \dot{\theta}_1 - C_1 C_2 S_3 \dot{\theta}_1 + C_1 C_2 S_2 \dot{\theta}_2 + S_1 S_2 S_3 \dot{\theta}_2),$

$c_{54} = -m_2 l_1 l_2 C_4 (C_1 C_3 S_2 \dot{\theta}_1 + S_1 S_2 S_3 \dot{\theta}_1 - C_1 C_2 S_3 \dot{\theta}_2 + C_2 C_3 S_1 \dot{\theta}_2),$

$c_{55} = -m_2 l_2^2 S_4 C_4 \dot{\theta}_4, c_{56} = -m_2 l_2^2 S_4 C_4 \dot{\theta}_3, c_{61} = 0, c_{62} = 0,$

$c_{63} = m_2 l_1 l_2 S_4 (C_1 C_2 C_3 \dot{\theta}_1 + C_2 S_1 S_3 \dot{\theta}_1 + C_1 C_2 S_3 \dot{\theta}_2 - C_3 S_1 S_2 \dot{\theta}_2),$

$c_{64} = m_2 l_1 l_2 (C_1 C_2 C_3 S_4 \dot{\theta}_2 + S_1 S_3 S_4 C_2 \dot{\theta}_2 - C_4 S_2 \dot{\theta}_2 + C_1 S_2 S_3 S_4 \dot{\theta}_1$

$- S_1 S_2 S_4 C_3 \dot{\theta}_1), c_{65} = m_2 l_2^2 S_4 C_4 \dot{\theta}_3, c_{66} = 0,$

$g_3 = (m_1 + m_2)gl_1 S_1 C_2, g_4 = (m_1 + m_2)gl_1 C_1 S_2,$

$g_5 = m_2 gl_2 S_3 C_4, g_6 = m_2 gl_2 C_3 S_4 \tag{2}$

where M_1 represent the mass of the trolley, the result of trolley's mass plus bridge' mass is set to M_2, m_1 represent the mass of hook, the mass of load is set to m_2. l_1 is the length of cable, l_2 is the distance from the hook to the load. θ_1, θ_2 are used to depict the swing of hook, θ_3 and θ_4 are used to depict the swing of load. Besides, for ease of reading, S_j is the abbreviation of $\sin\theta_j$ and C_j is the abbreviation of $\cos\theta_j (j = 1, 2, 3, 4)$. x and y denote the displacement variables of the trolley along the X-axis and the Y-axis. The force applied to the trolley along the X-axis, is set to F_x. Then, the force applied to the trolley along the Y-axis, is set to F_y. F_{rx}, F_{ry} describes the force of friction along the X-axis and the Y-axis, which are defined as follows:

$$F_{rx} = f_{rox} \tanh (\dot{x}/\delta_x) + \kappa_{rx} |\dot{x}| \dot{x} \tag{3}$$

$$F_{ry} = f_{roy} \tanh (\dot{y}/\delta_y) + \kappa_{ry} |\dot{y}| \dot{y} \tag{4}$$

where f_{rox}, f_{roy}, δ_x, δ_y represent the static friction coefficients, and κ_{rx} and κ_{ry} denote the viscous friction coefficients.

From (1), (2), it can be known that $M(q)$ is positive definite, and the anti-symmetric relation between the $M(q)$ and $C(q, \dot{q})$ is as follows:

$$\alpha^T \left[\frac{1}{2}\dot{M}(q) - C(q, \dot{q})\right] \alpha = 0, \forall \alpha \in R^6 \tag{5}$$

In general, the following assumption is reasonable:

– In practical application, the swing angle components studied in this paper have the following restrictions:

$$-\frac{\pi}{2} < \theta_1, \theta_2, \theta_3, \theta_4 < \frac{\pi}{2} \tag{6}$$

2.2   Control Objective

The control objective is that, on the one hand, the trolley can accurately reach the target position along the set trajectory, and on the other hand, it can effectively eliminate the swing angle of the hook and load. It can be elaborated as the following expressions:

$$\lim_{t\to\infty} x = x_r, \lim_{t\to\infty} y = y_r, \lim_{t\to\infty} \theta_1 = 0,$$
$$\lim_{t\to\infty} \theta_2 = 0, \lim_{t\to\infty} \theta_3 = 0, \lim_{t\to\infty} \theta_4 = 0 \tag{7}$$

where x_r, y_r denotes the reference trajectories of trolley. Regarding the reference trajectories x_r, y_r corresponding to x and y, the following conditions are generally guaranteed:

$$x_r, y_r, \dot{x}_r, \dot{y}_r \in L_\infty$$
$$x_r(0) = x_0, y_r(0) = y_0$$
$$\dot{x}_r(0) = 0, \dot{y}_r(0) = 0$$
$$\ddot{x}_r(0) = 0, \ddot{y}_r(0) = 0 \tag{8}$$

When $t \geq t_s$, it can be obtained that,

$$x_r(t) = x_d, y_r(t) = y_d,$$
$$\dot{x}_r(t) = 0, \dot{y}_r(t) = 0$$
$$\ddot{x}_r(t) = 0, \ddot{y}_r(t) = 0 \tag{9}$$

where x_0, y_0 denote the initial displacement values, x_d, y_d represent the desired positions, t_s is used to describe the settling time.

3   Controller Design

The energy equation of the crane system studied in this paper is described as follows

$$E = \frac{1}{2}\dot{q}^T M(q)\dot{q} + (m_1 + m_2) gl_1(1 - C_1C_2) + m_2gl_2(1 - C_3C_4) \tag{10}$$

Combining with Eq. (5), the expression of $\dot{E}$ can be obtained:

$$\dot{E} = \dot{q}^T M(q)\ddot{q} + \frac{1}{2}\dot{q}^T \dot{M}(q)\dot{q} + (m_1 + m_2) gl_1(S_1C_2\dot{\theta}_1 + C_1S_2\dot{\theta}_2)$$

$$+ m_2gl_2(S_3C_4\dot\theta_3 + C_3S_4\dot\theta_4)$$
$$= (F_x - F_{rx} - \Xi_1)\,\dot x + (F_y - F_{ry} - \Xi_2)\,\dot y$$
$$- \Xi_3\dot\theta_1 - \Xi_4\dot\theta_2 - \Xi_5\dot\theta_3 - \Xi_6\dot\theta_4 \tag{11}$$

where Ξ_1, Ξ_2, Ξ_3, Ξ_4 represent air frictions and ξ_1, ξ_2, ξ_3, ξ_4 denote friction-related parameters.

$$\Xi_1 = -\xi_1\dot x, \Xi_2 = -\xi_2\dot y, \Xi_3 = -\xi_3\dot\theta_1,$$
$$\Xi_4 = -\xi_4\dot\theta_2, \Xi_5 = -\xi_5\dot\theta_3, \Xi_6 = -\xi_6\dot\theta_4 \tag{12}$$

In order to improve the control performance, we built the following new signals by enhancing the coupling between the system state variables, and used them in the subsequent controller analysis and design.

$$\psi_x = x + \kappa_1 S_1C_2 + \kappa_2 S_3C_4 \tag{13}$$
$$\psi_y = y + \kappa_3 S_2 + \kappa_4 S_4 \tag{14}$$
$$e_{\psi x} = \psi_x - x_r = e_x + \kappa_1 S_1C_2 + \kappa_2 S_3C_4 \tag{15}$$
$$e_{\psi y} = \psi_y - y_r = e_y + \kappa_3 S_2 + \kappa_4 S_4 \tag{16}$$

where κ_1, κ_2, κ_3 and $\kappa_4 \in R$.

Hence, the tracking error vector can be expressed as follows:

$$\dot q_{e\psi} = \begin{bmatrix} \dot e_{\psi x} & \dot e_{\psi y} & \dot\theta_1 & \dot\theta_2 & \dot\theta_3 & \dot\theta_4 \end{bmatrix}^T \tag{17}$$

where $\dot e_{\psi x} = \dot x + (\kappa_1 S_1C_2 + \kappa_2 S_3C_4)' - \dot x_r, \dot e_{\psi y} = \dot y + (\kappa_3 S_2 + \kappa_4 S_4)' - \dot y_r$.

Based on the new error vector, the system energy equation can be rewritten as follows:

$$V_{E\Psi} = \frac{1}{2}\dot q_{e\psi}^T M \dot q_{e\psi} + (m_1 + m_2)\,gl_1(1 - C_1C_2) + m_2gl_2(1 - C_3C_4) \tag{18}$$

Substituting Eq. (2) and Eq. (17) into the derivative of $V_{E\Psi}$ with respect to time, the following expressions are obtained through mathematical calculation and sorting

$$\begin{aligned}
\dot V_{E\Psi} = &[F_x - F_{rx} - \Xi_1 + (M_1 + m_1 + m_2)(\kappa_1 S_1C_2 + \kappa_2 S_3C_4)'' \\
&- (M_1 + m_1 + m_2)\,\ddot x_r]\,\dot e_{\psi x} + [F_y - F_{ry} - \Xi_2 + (M_2 + m_1 + m_2) \\
&\times(\kappa_3 S_2 + \kappa_4 S_4)'' - (M_2 + m_1 + m_2)\,\ddot y_r]\,\dot e_{\psi y} \\
&+ [-\Xi_3 + (m_1 + m_2)l_1C_1C_2(\kappa_1 S_1C_2 + \kappa_2 S_3C_4)'' \\
&- (m_1 + m_2)l_1C_1C_2\,\ddot x_r]\,\dot\theta_1 \\
&+ [-\Xi_4 - (m_1 + m_2)l_1S_1S_2(\kappa_1 S_1C_2 + \kappa_2 S_3C_4)'' \\
&- (m_1 + m_2)l_1C_2(\kappa_3 S_2 + \kappa_4 S_4)'' + (m_1 + m_2)l_1S_1S_2\ddot x_r \\
&- (m_1 + m_2)l_1C_2\ddot y_r]\,\dot\theta_2 + [-\Xi_5 + m_2l_2C_3C_4(\kappa_1 S_1C_2 + \kappa_2 S_3C_4)'' \\
&- m_2l_2C_3C_4\,\ddot x_r]\,\dot\theta_3 + [-\Xi_6 - m_2l_2S_3S_4(\kappa_1 S_1C_2 + \kappa_2 S_3C_4)'' \\
&- m_2l_2C_4(\kappa_3 S_2 + \kappa_4 S_4)'' + m_2l_2S_3S_4\,\ddot x_r - m_2l_2C_4\ddot y_r]\,\dot\theta_4
\end{aligned} \tag{19}$$

where

$$\Upsilon_x = \left[\tanh\left(\tfrac{\dot{x}}{\delta_x}\right) \ |\dot{x}|\,x \ \dot{x} \ (\kappa_1 S_1 C_2 + \kappa_2 S_3 C_4)'' - \ddot{x}_r \right]^{\mathrm{T}} \tag{20}$$

$$\Upsilon_y = \left[\tanh\left(\tfrac{\dot{y}}{\delta_y}\right) \ |\dot{y}|\,y \ \dot{y} \ (\kappa_3 S_2 + \kappa_4 S_4)'' - \ddot{y}_r \right]^{\mathrm{T}} \tag{21}$$

$$\sigma_x = \left[f_{rox} \ \kappa_{rx} \ \xi_1 \ M_1 + m_1 + m_2 \right]^{\mathrm{T}} \tag{22}$$

$$\sigma_y = \left[f_{roy} \ \kappa_{ry} \ \xi_2 \ M_2 + m_1 + m_2 \right]^{\mathrm{T}} \tag{23}$$

$$\begin{aligned} \mathrm{H}_1 = -\xi_3\dot{\theta}_1^2 &+ [(m_1+m_2)l_1 C_1 C_2(\kappa_1 S_1 C_2 + \kappa_2 S_3 C_4)'' \\ &- (m_1+m_2)l_1 C_1 C_2 \ddot{x}_r]\,\dot{\theta}_1 \end{aligned} \tag{24}$$

$$\begin{aligned} \mathrm{H}_2 = -\xi_4\dot{\theta}_2^2 &+ [-(m_1+m_2)\,l_1 S_1 S_2(\kappa_1 S_1 C_2 + \kappa_2 S_3 C_4)'' \\ &- (m_1+m_2)l_1 C_2(\kappa_3 S_2 + \kappa_4 S_4)'' \\ &+ (m_1+m_2)l_1 S_1 S_2 \ddot{x}_r - (m_1+m_2)\,l_1 C_2 \ddot{y}_r]\,\dot{\theta}_2 \end{aligned} \tag{25}$$

$$\mathrm{H}_3 = -\xi_5\dot{\theta}_3^2 + \left[m_2 l_2 C_3 C_4\,(\kappa_1 S_1 C_2 + \kappa_2 S_3 C_4)'' - m_2 l_2 C_3 C_4 \ddot{x}_r \right]\dot{\theta}_3 \tag{26}$$

$$\begin{aligned} \mathrm{H}_4 = -\xi_6\dot{\theta}_4^2 &+ [-m_2 l_2 S_3 S_4\,(\kappa_1 S_1 C_2 + \kappa_2 S_3 C_4)'' - m_2 l_2 C_4(\kappa_3 S_2 + \kappa_4 S_4)'' \\ &+ m_2 l_2 S_3 S_4\,\ddot{x}_r - m_2 l_2 C_4 \ddot{y}_r]\,\dot{\theta}_4 \end{aligned} \tag{27}$$

Inspired by Eq. (19), the following control laws can be constructed:

$$F_x = -k_{px}e_{\psi x} - k_{dx}\dot{e}_{\psi x} + \Upsilon_x^{\mathrm{T}}\hat{\sigma}_x \tag{28}$$

$$F_y = -k_{py}e_{\psi y} - k_{dy}\dot{e}_{\psi y} + \Upsilon_y^{\mathrm{T}}\hat{\sigma}_y \tag{29}$$

where k_{px}, k_{py}, k_{dx}, k_{dy} are undetermined control parameters, $\hat{\sigma}_x$, $\hat{\sigma}_y$ denotes the estimators of σ_x, σ_y and the specific expressions are as follows:

$$\hat{\sigma}_x = \left[\hat{f}_{rox} \ \hat{\kappa}_{rx} \ \hat{\xi}_1 \ M_1 + \widehat{m_1 + m_2} \right]^{\mathrm{T}} \tag{30}$$

$$\sigma_y = \left[\hat{f}_{roy} \ \hat{\kappa}_{ry} \ \hat{\xi}_2 \ M_2 + \widehat{m_1 + m_2} \right]^{\mathrm{T}} \tag{31}$$

Then, the adaptive laws are designed as follows:

$$\dot{\hat{\sigma}}_x = -\mathrm{A}^{-1}\Upsilon_x \dot{e}_{\psi x},\ \dot{\hat{\sigma}}_y = -\mathrm{B}^{-1}\Upsilon_y \dot{e}_{\psi y} \tag{32}$$

$$\mathrm{A} = diag\left\{ a_1\ a_2\ a_3\ a_4 \right\} \in R^{4\times 4} \tag{33}$$

$$\mathrm{B} = diag\left\{ b_1\ b_2\ b_3\ b_4 \right\} \in R^{4\times 4} \tag{34}$$

However, in actual application, the velocity signals are not measurable during the crane operation, which is also the weakness of the controller in Eqs. (28), (29). Therefore, we construct auxiliary functions ϖ_x and ϖ_y containing the velocity signals and introduce it into the controller in Eqs. (28), (29). Whereupon a novel adaptive output feedback control method, which can handle the aforementioned issue, is presented.

$$F_x = -k_{px}e_{\psi x} - k_{dx}\varpi_x + \Upsilon_x^{\mathrm{T}}\hat{\sigma}_x \tag{35}$$

$$F_y = -k_{py}e_{\psi y} - k_{dy}\varpi_y + \Upsilon_y^{\mathrm{T}}\hat{\sigma}_y \tag{36}$$

where

$$\varpi_x = \lambda_x + k_{dx}e_{\psi x}, \dot{\lambda}_x = -k_{dx}\left(\lambda_x + k_{dx}e_{\psi x}\right) \tag{37}$$

$$\varpi_y = \lambda_y + k_{dy}e_{\psi y}, \dot{\lambda}_x = -k_{dy}\left(\lambda_y + k_{dy}e_{\psi y}\right) \tag{38}$$

$$\dot{\varpi}_x = -k_{dx}\varpi_x + k_{dx}\dot{e}_{\psi x} \tag{39}$$

$$\dot{\varpi}_y = -k_{dy}\varpi_y + k_{dy}\dot{e}_{\psi y} \tag{40}$$

4   Results and Discussion

To further conform the superiority of the control strategy, as mentioned in Eqs. (35), (36), in terms of trolley positioning and swing angles reduction, the MAT-LAB is used for simulation verification and analysis.

4.1   Simulation Conditions

Firstly, the dynamic model given in Eq. (1) is operated by the proposed controller. When selecting these control gains, the first step is to adjust the control gains $k_{px}, k_{dx}, k_{py}, k_{dy}$ on the basis of PD controller, and then fine tune the control gains $\kappa_1, \kappa_2, \mathrm{A}, \mathrm{B}$. After repeated trial and error, the controller gains used in the simulation are selected as follows:

$$k_{px} = 8, k_{dx} = 6, k_{py} = 8, k_{dy} = 10$$
$$\kappa_1 = -0.27, \kappa_2 = -0.25$$
$$\mathrm{A} = diag\left\{0.01\ 0.01\ 0.01\ 0.01\right\}$$
$$\mathrm{B} = diag\left\{0.01\ 0.01\ 0.01\ 0.01\right\} \tag{41}$$

The target positions of the trolley are set as $x_d = 0.3\,[m]$, $y_d = 0.3\,[m]$ $t_s = 3[s]$, and the initial positions x_0, y_0 are set to zero. The physical parameters of the crane model are set as follows: $M_1 = 0.5[\mathrm{kg}]$, $M_2 = 2.5[\mathrm{kg}]$, $m_1 = 0.5[\mathrm{kg}]$, $m_2 = 0.5\,[\mathrm{kg}]$, $l_1 = 0.4[\mathrm{m}]$, $l_2 = 0.3[\mathrm{m}]$.

4.2   Comparative Simulations

In this subsection, in order to verify the effectiveness of the proposed control strategy, the comparative simulations are carried out.
    (1) Sliding mode controller

$$F = \left(P^T P\right)^{-1} P^T \left(R + \ddot{q} - \Lambda \dot{e} - ks - \mu \tanh\left(s\right)\right) \tag{42}$$

with $s = \dot{e} + \beta\dot{e}$ and $e = q - q_d$ representing the chosen sliding surface and error matrix respectively, where $q = \begin{bmatrix} x\ y\ \theta_1\ \theta_2\ \theta_3\ \theta_4 \end{bmatrix}^T$, $q_d = \begin{bmatrix} x_d\ y_d\ 0\ 0\ 0\ 0 \end{bmatrix}^T$. Meanwhile, Λ is a positive gain matrix and k, μ are undetermined parameters.

After carefully selecting parameters by trial and error, the following values can be obtained: $\Lambda = diag\{0.085, 0.1, 1, 1, 1, 1\}$, $k = \mu = 5$. P and R are the auxiliary matrix functions in Eq. (43), which are defined as:

$$P = \begin{bmatrix} p_{11} & p_{21} & p_{31} & p_{41} & p_{51} & p_{61} \\ p_{12} & p_{22} & p_{32} & p_{42} & p_{52} & p_{62} \end{bmatrix}^T \tag{43}$$
$$R = \begin{bmatrix} r_{11} & r_{21} & r_{31} & r_{41} & r_{51} & r_{61} \end{bmatrix}^T$$

with

$$p_{11} = \frac{1}{M_1}, p_{21} = 0, p_{31} = -\frac{1}{M_2 l_1}, p_{41} = 0, p_{51} = 0, p_{61} = 0,$$

$$p_{12} = 0, p_{22} = \frac{1}{M_2}, p_{32} = 0, p_{42} = -\frac{1}{M_2 l_1}, p_{52} = 0, p_{62} = 0,$$

$$r_{11} = \frac{(m_1 g\theta_1 + m_2 g\theta_1)}{M_1}, r_{21} = \frac{(m_1 g\theta_2 + m_2 g\theta_2)}{M_2},$$

$$r_{31} = \frac{(M_1 + m_1 + m_2)m_1 g\theta_1 + m_1 m_2 g(\theta_1 - \theta_3)}{M_1 m_1 l_1},$$

$$r_{41} = \frac{(M_2 + m_1 + m_2)m_1 g\theta_2 + M_2 m_2 g(\theta_2 - \theta_4)}{M_2 m_1 l_1},$$

$$r_{51} = \frac{(m_1 + m_2) g (\theta_1 - \theta_3)}{m_1 l_2},$$

$$r_{61} = \frac{(m_1 + m_2) g (\theta_2 - \theta_4)}{m_1 l_2} \tag{44}$$

(2) LQR controller

$$F_x = -k_{px}e_x - k_{dx}\dot{x} - k_1\theta_1 - k_2\theta_3 - k_3\dot{\theta}_1 - k_4\dot{\theta}_3 + F_{rx},$$
$$F_y = -k_{py}e_y - k_{dy}\dot{y} - k_5\theta_2 - k_6\theta_4 - k_7\dot{\theta}_2 - k_8\dot{\theta}_4 + F_{ry}, \tag{45}$$

with k_{px}, k_{py}, k_{dx}, k_{dy}, k_a, k_b, k_c, k_d, k_e, k_f, k_g, $k_h \in R$ denote control gains, which are calculated $k_{px} = 11.3137$, $k_{py} = 11.3137$, $k_{dx} = 18.5403$, $k_{dy} = 22.9924$, $k_a = -76.0345$, $k_b = -15.2300$, $k_c = 40.6143$, $k_d - 0.1772$, $k_e = -44.4926$, $k_f = -17.7791$, $k_g = 21.5435$ and $k_h = 1.2262$.

In order to intuitively demonstrate the superiority of the proposed controller in trolley tracking and positioning and restraining the load swing angles, the simulation results of actuated state components x, y, underactuated state components θ_1, θ_2, θ_3, θ_4, and input force F_x, F_y, when the three controllers act on the crane are all reflected in Fig. 2. The sub-figure in the first row of Fig. 2 describes the tracking and positioning performance of the trolley. Through comparative analysis, the conclusion can be drawn that the proposed controller can

drive the trolley to reach the set position significantly faster than the other two control methods. The second and third rows of Fig. 2 display the simulation results of the swing angles of the crane during operation. Under the control of the proposed control strategy, when the trolley reaches the target position, the swing angles are also suppressed to 0. Although the swing angles can also be eliminated by the other two controllers, they takes longer time because of their longer positioning time. In addition, when adopting the proposed controller, the amplitude of the load swing angles are smaller than that of the other two controllers. In conclusion, the proposed control strategy achieves better performance than the other two control methods in terms of trolley positioning, swing angles elimination.

4.3   Robust Performance

In order to verify the robustness of the proposed controller, we carried out the following three sets of simulation to reflect the control performance under the perturbation of the system model parameters and the non-zero initial swing angle. Meanwhile, The control parameters in the following sets of simulations are all the same values in Eq. (42). For easy analysis, the parameter changes are placed together with the original image In order to facilitate the analysis, the figure with the changed parameters and the original picture are plotted together.

In the first set of simulation, we obtained the simulation results presented in Fig. 3 by changing the load mass from 0.5 [kg] to 1 [kg], 1.5 [kg]. It can be the control performance of the proposed controller is basically the same. Next, we changed the rope length l_2 to 0.2[m], 0.4[m] and got the conclusion that different l_2 can not impose the influence on control performance. The results reveal that the control method has strong robustness to the changes of crane model parameters.

Finally, non-zero initial value of double-pendulum load sway angles, which were set as $\theta_1(0) = -4.6[deg]$, $\theta_2(0) = -4.6[deg]$, $\theta_3(0) = -4.6[deg]$, and $\theta_4(0) = -4.6[deg]$, were also considered in this study. It can be seen intuitively from Fig. 5 that the controller can still maintain an excellent control effect which is shown in the positioning time of the trolley and the elimination effect of the swing angles are basically unchanged when existing non-zero initial swing angle.
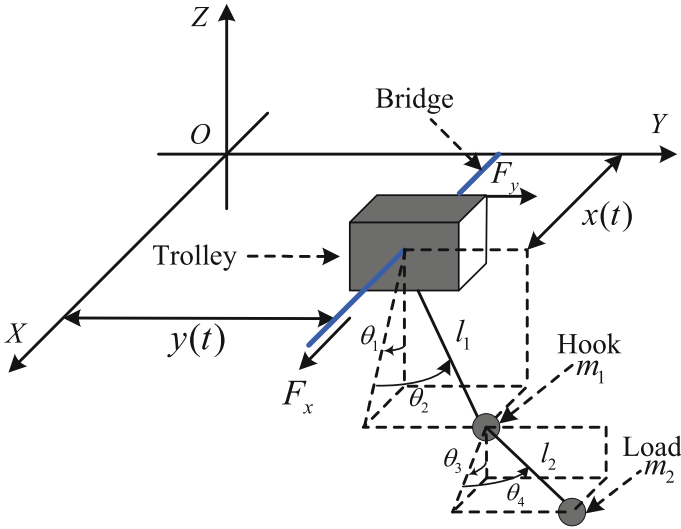
Fig. 1. Three-dimensional overhead cranes with double-pendulum effect model
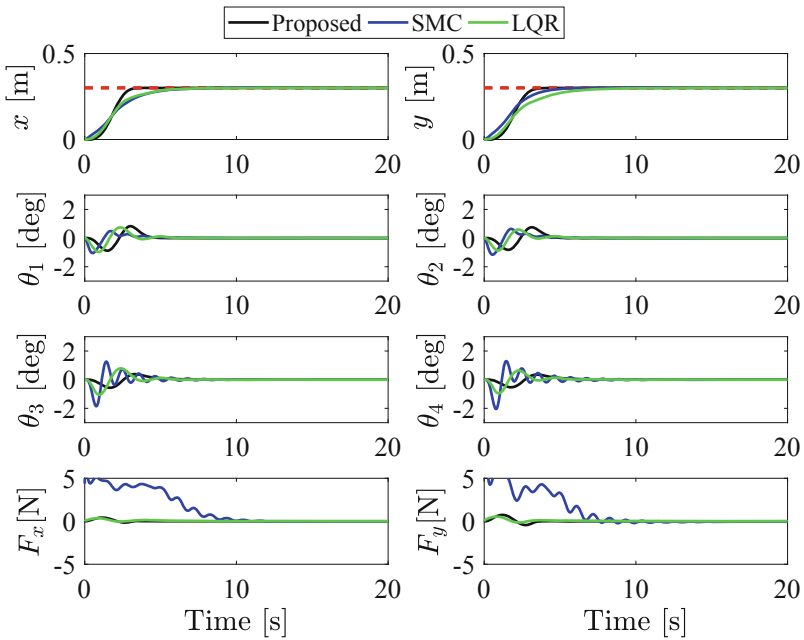

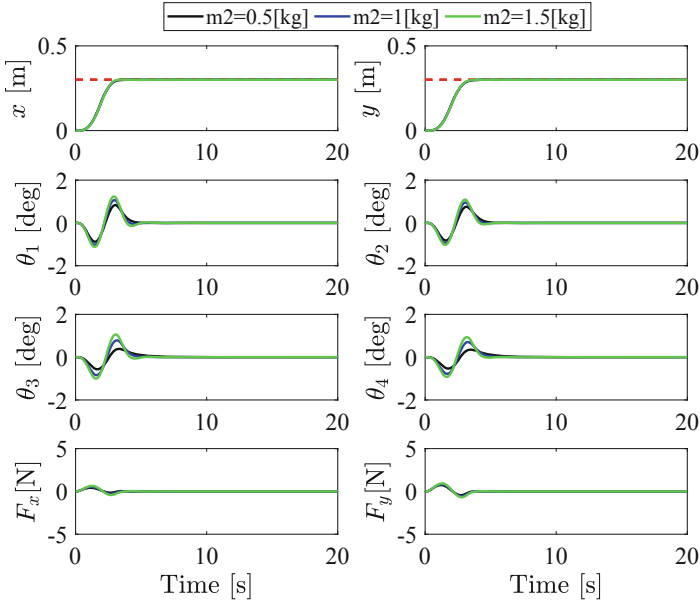**Fig. 2.** Comparative simulation results

Fig. 3. Simulation results with different load mass
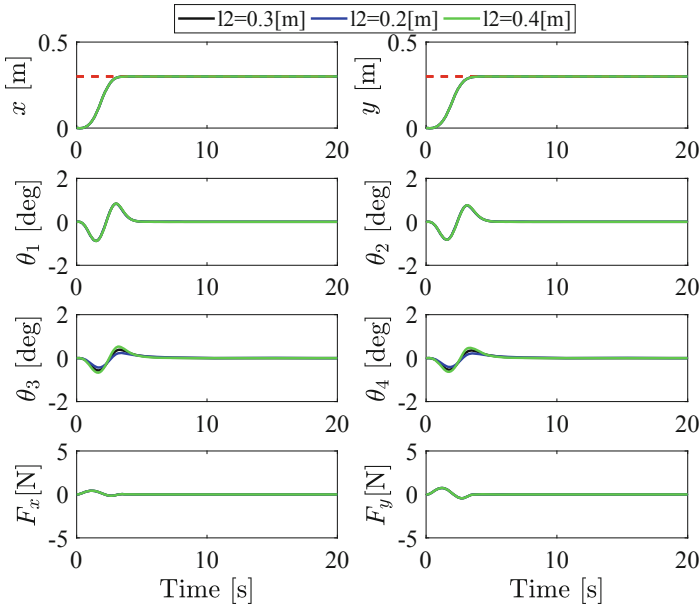

Fig. 4. Simulation results with different rope length
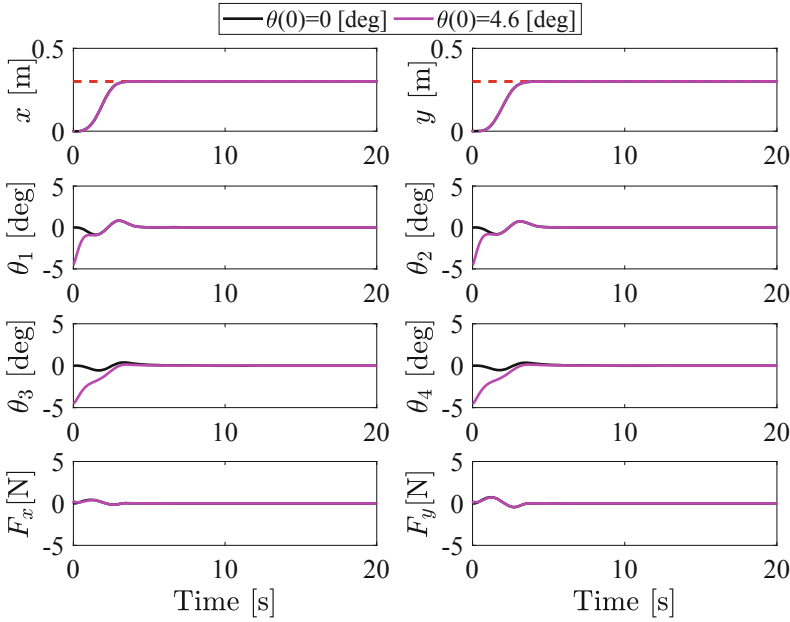
Fig. 5. Simulation results with non-zero initial hook and load sway angles

5   Conclusion

Aiming at the complex dynamics model of the three-dimensional double pendulum overhead crane, an improved adaptive tracking controller is derived. By constructing new signals to increase the coupling relationship of the state vector, all the controlled state vectors are included in the controller. In addition, auxiliary functions are designed to handle the issue that the velocity signals cannot be measured. A series of simulation results intuitively confirmed the feasibility and robustness of the proposed controller.

References

1. Ramli L, Mohamed Z, Abdullahi A, Jaafar H, Lazim I (2017) Control strategies for crane systems: a comprehensive review. Mech Syst Signal Process 95:1–23
2. Fang Y, Ma B, Wang P, Zhang X (2012) A motion planning-based adaptive control method for an underactuated crane system. Control Syst Technol IEEE Trans 20(1):241–248
3. Sun N, Fang Y (2014) An efficient online trajectory generating method for under-actuatedcrane systems. Int J Robust Nonlinear Control 24(11):1653–1663

4. Peng H, Shi B, Wang X, Li C (2019) Interval estimation and optimization for motion trajectory of overhead crane under uncertainty. Nonlinear Dyn 96(2):1693–1715. https://doi.org/10.1007/s11071-019-04879-w

5. Maghsoudi M, Mohamed Z, Sudin S, Buyamin S, Jaafar H, Ahmad S (2017) An improved input shaping design for an efficient sway control of a nonlinear 3d overhead crane with friction. Mech Syst Signal Process 92:364–378

6. Ramli L, Mohamed Z, Jaafar H (2018) A neural network-based input shaping for swing suppression of an overhead crane under payload hoisting and mass variations. Mech Syst Signal Process 107:484–501

7. Alghanim K, Mohammed A, Andani M (2019) An input shaping control scheme with application on overhead cranes. Int J Nonlinear Sci Numer Simul 20(5):561–573

8. Chwa D (2017) Sliding mode control-based robust finite-time anti-sway tracking control of 3-d overhead cranes. IEEE Trans Ind Electron 64(8):6775–6784

9. Lu B, Fang Y, Sun N (2017) Sliding mode control for underactuated overhead cranes suffering from both matched and unmatched disturbances. Mechatronics 47:116–125

10. Gu X, Xu W (2020) Moving sliding mode controller for overhead cranes suffering from matched and unmatched disturbances. Trans Inst Meas Control 014233122092210

11. Zhang M, Zhang Y, Ji B, Ma C, Cheng X (2020) Adaptive sway reduction for tower crane systems with varying cable lengths. Autom Constr 119:103342

12. Chen H, Fang Y, Sun N (2019) An adaptive tracking control method with swing suppression for 4-dof tower crane systems. Mech Syst Signal Process 123:426–442

13. Liu P, Yu H, Cang S (2019) Adaptive neural network tracking control for underactuated systems with matched and mismatched disturbances. Nonlinear Dyn 98(2):1447–1464. https://doi.org/10.1007/s11071-019-05170-8

14. Zhang M, Zhang Y, Ji B (2019) Modeling and energy-based sway reduction control for tower crane systems with double-pendulum and spherical-pendulum effects. Measur Control 53(1–2):141–150

15. Ouyang H, Tian Z, Yu L, Zhang G (2020) Load swing rejection for double-pendulum tower cranes using energy-shaping-based control with actuator output limitation. ISA Trans 101:246–255

16. Chen H, Sun N (2020) Nonlinear control of underactuated systems subject to both actuated and unactuated state constraints with experimental verification. IEEE Trans Ind Electron 67(9):7702–7714

17. Guo B, Chen Y (2020) Fuzzy robust fault-tolerant control for offshore ship-mounted crane system. Inf Sci 526:119–132

18. Qian D, Tong S, Lee SG (2016) Fuzzy-logic-based control of payloads subjected to double-pendulum motion in overhead cranes. Autom Constr 65:133–143

19. Yang T, Sun N, Chen H, Fang Y (2020) Neural network-based adaptive antiswing control of an underactuated ship-mounted crane with roll motions and input dead zones. IEEE Trans Neural Netw Learn Syst 31(3):901–914

20. Li F, Zhang C, Sun B (2019) A minimum-time motion online planning method for 7 underactuated overhead crane systems. IEEE Access 99(7):54586–54594

21. Ji Y, Leite F (2020) Optimized planning approach for multiple tower cranes and material supply points using mixed-integer programming. J Constr Eng Manage 146(3):1–11

22. Zhang M, Ma X, Chai H, Rong X, Tian X, Li Y (2016) A novel online motion planning method for double-pendulum overhead cranes. Nonlinear Dyn 85(2):1079–1090. https://doi.org/10.1007/s11071-016-2745-x

23. Wu X, Xu K, He X (2020) Disturbance-observer-based nonlinear control for overhead cranes subject to uncertain disturbances. Mech Syst Signal Process 139:106631.1–106631.18
24. Zhang M, Zhang Y, Ouyang H, Ma C, Cheng X (2020) Adaptive integral sliding mode control with payload sway reduction for 4-dof tower crane systems. Nonlinear Dyn 99(4):2727–2741
25. Le V-A, Le H-X, Nguyen L, Phan M-X (2019) An efficient adaptive hierarchical sliding mode control strategy using neural networks for 3D overhead cranes. Int J Autom Comput 16(5):614–627. https://doi.org/10.1007/s11633-019-1174-y
26. Ouyang H, Zhao B, Zhang G (2021) Enhanced-coupling nonlinear controller design for load swing suppression in three-dimensional overhead cranes with double-pendulum effect. https://doi.org/10.1016/j.isatra.2021.01.009
27. Ouyang H, Zhao B, Zhang G (2021) Swing reduction for double-pendulum three-dimensional overhead cranes using energy-analysis-based control method https://doi.org/10.1002/rnc.5466